Engineering Giant Excitonic Coupling in Bioinspired, Covalently Bridged BODIPY Dyads

Sara Ansteatt,[†] Brian Uthe,[‡] Bikash Mandal,[§] Rachel Gelfand,[‡] Barry D. Dunietz,*[,§] Matthew Pelton,*[,†,‡] and Marcin Ptaszek*[,†]

[†]Department of Chemistry and Biochemistry
‡Department of Physics
University of Maryland, Baltimore County
1000 Hilltop Circle
Baltimore, MD 21250

[§]Department of Chemistry and Biochemistry
Kent State University
Kent, OH 44242

TOC

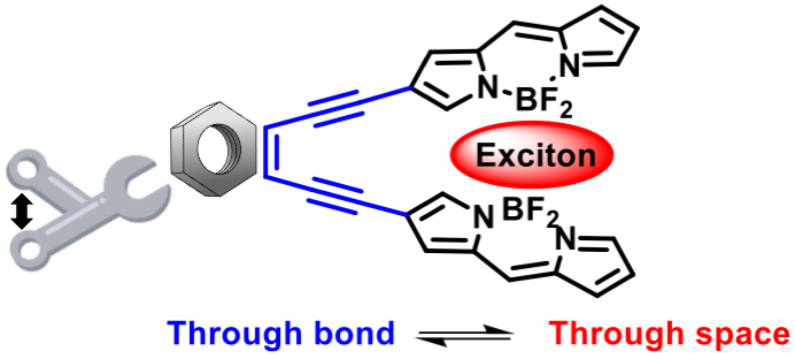

Abstract

Strong excitonic coupling in photosynthetic systems is believed to enable efficient light absorption and quantitative charge separation, motivating the development of artificial multi-chromophore arrays with equally strong or even stronger excitonic coupling. However, large excitonic coupling strengths have typically been accompanied by fast non-radiative recombination, limiting the potential of the arrays for solar energy conversion as well as other applications such as fluorescent labeling. Here, we report giant excitonic coupling leading to broad optical absorption in bioinspired BODIPY dyads that have high photostability, excited-state lifetimes at the nanosecond scale, fluorescence quantum yields of nearly 50%. Through the synthesis, spectroscopic characterization, and computational modeling of a series of dyads with different linking moieties, we show that the strongest coupling is obtained with diethynylmaleimide linkers, for which the coupling occurs through space between BODIPY units with small separations and slipped co-facial orientations. Other linkers allow for broad tuning of both the relative through-bond and through-space coupling contributions and the overall strength of interpigment coupling, with a tradeoff observed in general between the strength of the two coupling mechanisms. These findings open the door to the synthesis of molecular systems that function effectively as light-harvesting antennas and as electron donors or acceptors for solar energy conversion.

Introduction

Strongly interacting chromophores are key components in photosynthetic light-harvesting antennas[1-5] and photosynthetic reaction centers.[1,5] It has long been argued that electronic inter-pigment interactions play a pivotal role in the efficient light harvesting and ultrafast, nearly quantitative charge separation accomplished by natural photosynthetic systems.[5-19] This has inspired a growing interest in producing artificial multi-chromophoric arrays with strong inter-pigment electronic interactions that mimic the advantages of natural systems for developing diverse functional photonic materials.[20-44]

Designing arrays with strong excitonic coupling and long excited-state lifetimes requires an understanding of and control over the coupling mechanisms, as numerous processes may result in quenching of the excited state, such as increase in non-radiative rate constants,[44,45] symmetry-breaking charge transfer,[47,48] and excimer formation.[49,50] In synthetic arrays, as in natural systems, excitonic coupling between adjacent chromophores can occur both by interactions between transition dipole moments (long-range excitonic coupling) and by spatial overlap of π-orbitals (short-range excitonic coupling).[20,21,51,52] This "through-space" coupling has the effect on the absorption spectra,[20,51] with absorption peaks shifting to higher energies for face-to-face arrangements of the chromophores (H-aggregates) and peaks shifting to lower energies for head-to-tail arrangements (J-aggregates). Slipped co-facial arrangements, which break the symmetry of H-aggregates, can produce two new absorption peaks in place of the original one, with maxima located at both shorter and longer wavelengths, thus enabling broadband optical absorption. Moreover, the short-range excitonic coupling significantly modifies the ground-state electronic structure of individual chromophores.[46,53,54] In synthetic arrays where chromophores are connected by molecular linkers, "through-bond" coupling is also possible, due to electronic π-conjugation through conjugated linking moieties, which further modifies the ground-state electronic structure of chromophores.[46,54]

A variety of chromophores have been studied for such synthetic arrays, including porphyrins,[22,23,37,38,46,54] acenes,[32,35,36,39,41] rylenediimides,[25,30,40] squaraines,[34,42] and (mero)cyanines.[43,44] Coupling strengths (calculated as a half of the energy between the maxima in the absorption band) as large as 1488 cm^{-1} have been obtained using cyanines.[44] In this study, we employ a BODIPY derivative. BODIPYs are characterized by intense absorbance around 500 nm that can by significantly red-shifted by chemical means up to 700 nm, and feature relatively high stability and facile synthesis.[55-57] BODIPY derivatives have been explored in arrays for solar energy conversion both as light-harvesting units and as redox-active components.[56,57] Multiple arrays containing BODIPYs have been studied, including strongly π-conjugated dyads,[58-64] co-facial dyads,[49,50,65,66] directly-linked dyads,[47,48,67-69] and cyclic BODIPY arrays.[70-74] Directly-linked dyads have shown excitonic coupling as large as 1313 cm^{-1} (2626 cm^{-1} separation of absorption-band maxima).[67] Numerous photochemical processes have been reported for dyads containing BODIPY, including symmetry-breaking photoinduced electron transfer[47,48] and singlet fission.[69]

The complexity of the various coupling mechanisms, all of which can operate simultaneously, means that optimization of chromophoric arrays must be approached empirically, through a combination of organic synthesis, spectroscopic studies, and computational analysis. In this contribution, we apply this approach to a series of dyads with a range of conjugated and non-conjugated chemical linkers that provide a range of co-facial and non-co-facial arrangements.

For our BODIPY dyads, we find that maximizing the strength of the through-space interaction, by reducing the separation between the chromophores, comes at the cost of weakening the through-bond interaction, due to increased geometrical strain. The greatest observed coupling strength, which is manifested by observed splitting of the absorption band of 2644 cm^{-1}, was found in dyads linked by diethynylmaleimide for which the excitonic coupling is predominantly through space. All the arrays are photostable and have excited-state lifetimes in the nanosecond range,

giving them the potential to serve as energy or charge donors in bioinspired molecular systems for solar energy conversion.

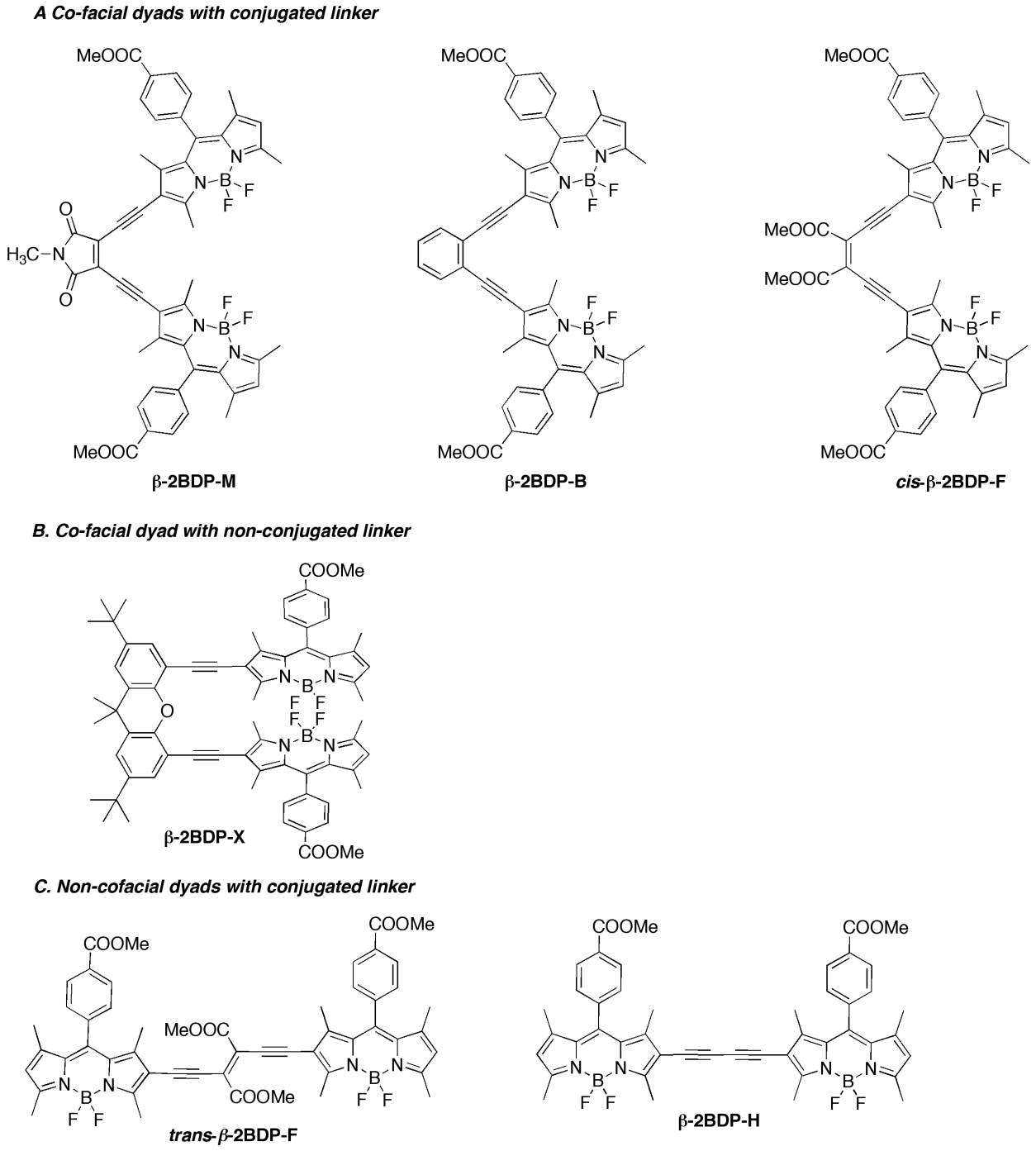

Chart 1. BODIPY dyads studied in this paper.

Results

Molecular Design. Chart 1 shows the series of dyads that we studied. In each dyad, the BODIPY subunits are connected through the *β* site (the 2-position of BODIPY), aligning the linker along the $S_0 \rightarrow S_1$ transition dipole moment (see Chart 2).[75] The first set of compounds comprises dyads where a conjugated *cis* enediyne linker is connected to the *β*-position, resulting in a slipped co-facial geometry of the BODIPY subunits. We anticipate that *cis*-enediyne linker provides at the same time co-facial arrangement of chromophores as well as through-bond π-conjugation. Three different enediyne linkers are investigated: diethynylmaleimide (**β-2BDP-M**), 1,2-diethynylphenyl (**β-2BDP-B**), and 2,3-diethynylmaleate (**β-2BDP-F**). We found that **β-2BDP-F** was synthesized in its *trans* isomeric form, which does not have a co-facial alignment of the BODIPY subunits. However, irradiation of ***trans*-β-2BDP-F** at the maximum of its absorption band (595 nm) resulted in a rapid change of the absorption band into two new peaks with maxima at 520 and 567 nm (see Figure S1).[47] The spectrum reached a photostationary state after approximately 5 min. We attribute these changes to *trans-cis* photoisomerization into a form with slipped co-facial alignment of the chromophores. The resulting ***cis*-β-2BDP-F** is stable and does not show any noticeable changes in absorption when stored in the dark for weeks.

The ***trans*-β-2BDP-F** form provides a sample where the BODIPY subunits are joined with a conjugated linker but are spatially separated and should not exhibit any through-space interaction. As a second molecule of this type, we synthesized dyads with a butadiyne linker (**β-2BDP-H**). We also synthesized dyads where the BODIPY subunits are arranged in a slipped co-facial geometry but are linked by non-conjugated diethynylxanthene (**β-2BDP-X**). Finally, we examined **β-BDP-Ph** as a benchmark monomer (see Chart 2).

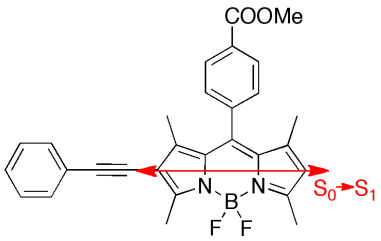

β-BDP-Ph

Chart 2. Structure of benchmark monomer **β-BDP-Ph**. The orientation of the $S_0 \rightarrow S_1$ transition dipole moment is shown as a red arrow.

Table 1 summarizes the systems that were synthesized for this study.

Table 1. Summary of BODIPY dyads studied, the linker molecule connecting the BODIPY molecules, the nature of the linking molecule (conjugated or non-conjugated), and the arrangement of the BODIPY units (slipped co-facial or non-co-facial). The following letters were used for linker designation: M – maleimide, B – *o*-phenylene, F – fumarate, X – xanthene, H - butadiyne

Dyad	Linker	Linker type	Arrangement
β-2BDP-M	maleimide	conjugated	co-facial
β-2BDP-B	phenyl	conjugated	co-facial
***cis*-β-2BDP-F**	maleate	conjugated	co-facial
β-2BDP-X	xanthene	non-conjugated	co-facial
***trans*-β-2BDP-F**	maleate	conjugated	non-co-facial
β-2BDP-H	butadiyne	conjugated	non-co-facial
β-BDP-Ph	(Benchmark monomer)		

Synthesis. The key building block for preparation of all dyads is **β-BDP-EH**, whose synthesis is presented in Scheme 1. As a first step, iodination of **β-BDP-1**[76] with I_2/HIO_3 using a published protocol[60,77] provided **β-BDP-I** at 77% yield. Subsequent Sonogashira reaction with

TMS-protected acetylene provided **β-BDP-TMS** at 85% yield, which provides, upon deprotection, **β-BDP-EH** at 83% yield.

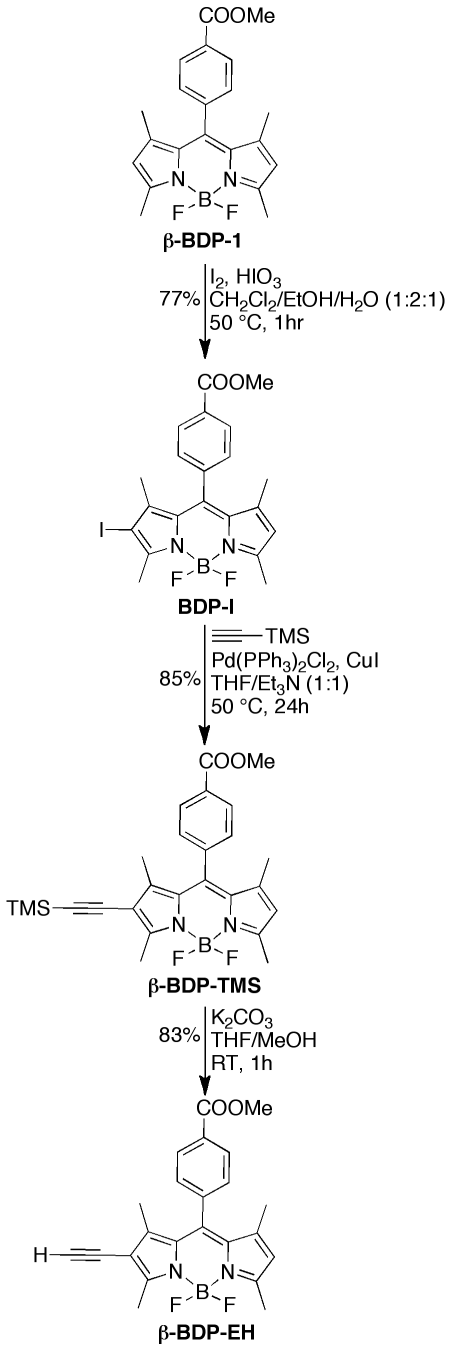

Scheme 1. Synthesis of **β-BDP-EH**.

Table 2. Synthesis of BODIPY dyads.

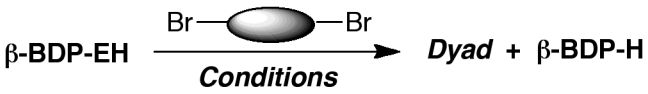

Entry	Br—⬭—Br	*Conditions*	**Dyad**	Yield [a]

1	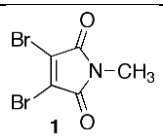	$Pd_2(dba)_3$, P(*o*-tolyl)$_3$ toluene/Et_3N (5:1) 60 °C, 24 hr	**β-2BDP-M**	45% (21%) [b]
2	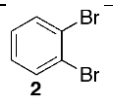	$Pd_2(dba)_3$, P(*o*-tolyl)$_3$ Toluene/Et_3N (5:1) 60 °C, 24 hr	**β-2BDP-B**	61%
3	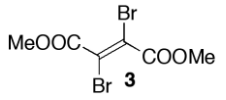	$Pd_2(dba)_3$, P(*o*-tolyl)$_3$ Toluene/Et_3N (5:1) 60 °C, 24 hr, dark	***trans*-β-2BDP-F**	61%
4	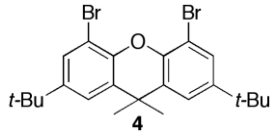	$Pd_2(dba)_3$, P(*o*-tolyl)$_3$ Toluene/Et_3N (5:1) 60 °C, 18hr	**β-2BDP-X**	75%

[a] Formation of varied (in most cases unquantified) amount of **β-BDP-H** was detected for each of these reactions. [b] Yield of **β-BDP-H**.

Dyads were prepared by the Sonogashira reaction of **β-BDP-EH** with corresponding dibromides (Table 2). Initially, we applied the standard conditions for the Cu(I)-catalyzed Sonogashira reaction (i.e. $Pd(PPh_3)_2Cl_2$, CuI, THF/Et_3N); however, under these conditions, dyads were obtained in low yield and the symmetrical dyad **β-2BDP-H** was isolated as the main product. We therefore employed Cu(I)-free conditions, developed previously for porphyrins,[78] which provided the desired dyads with satisfactory yield (some unquantified amount of **β-2BDP-H** was still isolated in each reaction). Specifically, reaction of **β-BDP-EH** with dibromomaleimide **1** under copper-free conditions [$Pd_2(dba)_3$, P(*o*-tolyl)$_3$, toluene/Et_3N (5:1), at 65 °C] provided **β-2BDP-M** at 45% yield, while reaction with *o*-dibromobenzene **2** under the same conditions provided **β-2BDP-B** at 61% yield. Fumarate-linked dyad ***trans*-β-2BDP-F** was synthesized in reaction of **β-BDP-EH** with *trans*-dibromofumarate **3**,[79,80] which provides ***trans*-β-2BDP-F** at 61% yield. In this case, both reaction and purification were carried out in the dark to avoid possible *trans-cis* isomerization. **β-2BDP-H** was isolated as a side product in non-optimized attempted synthesis of **β-2BDP-B**. Finally, **β-2BDP-X** was synthesized by Sonogashira reaction of **β-BDP-EH** with 1,8-dibromoxanthene **4**, at relatively high yield (75%).

The dyads were characterized by ^{1}H and ^{13}C NMR. Spectra are consistent with proposed structures. Mass spectroscopy shows m/z consistent with the expected structures.

Structure and optical properties. Figure 1 shows the optical absorption and emission spectra of the dyads that are expected to have a slipped co-facial arrangement of the BODIPY units (Spectra for the non-co-facial dyads are shown in Figure S2). Also shown are the three-dimensional structures of these dyads, as determined using density-functional-theory (DFT) calculations. The calculations confirm the expected slipped co-facial arrangement of the pigments. The mutual orientation of BODIPY transition dipole moments in dyads also feature a displacement from the parallel orientation, necessary for the H-coupling. This displacement, quantified as a deviation from parallel orientation of transition dipole moments increases in order of **β-2BDP-M** < **β-2BDP-X** < **β-2BDP-B** < ***cis*-β-2BDP-F**. The same trend is observed for the deviation from parallel orientation of mean planes of BODIPY subunit (See Table S1). Overall, in **2BDP-M** BODIPY mean planes and transition dipole moments nearly perfectly parallel.

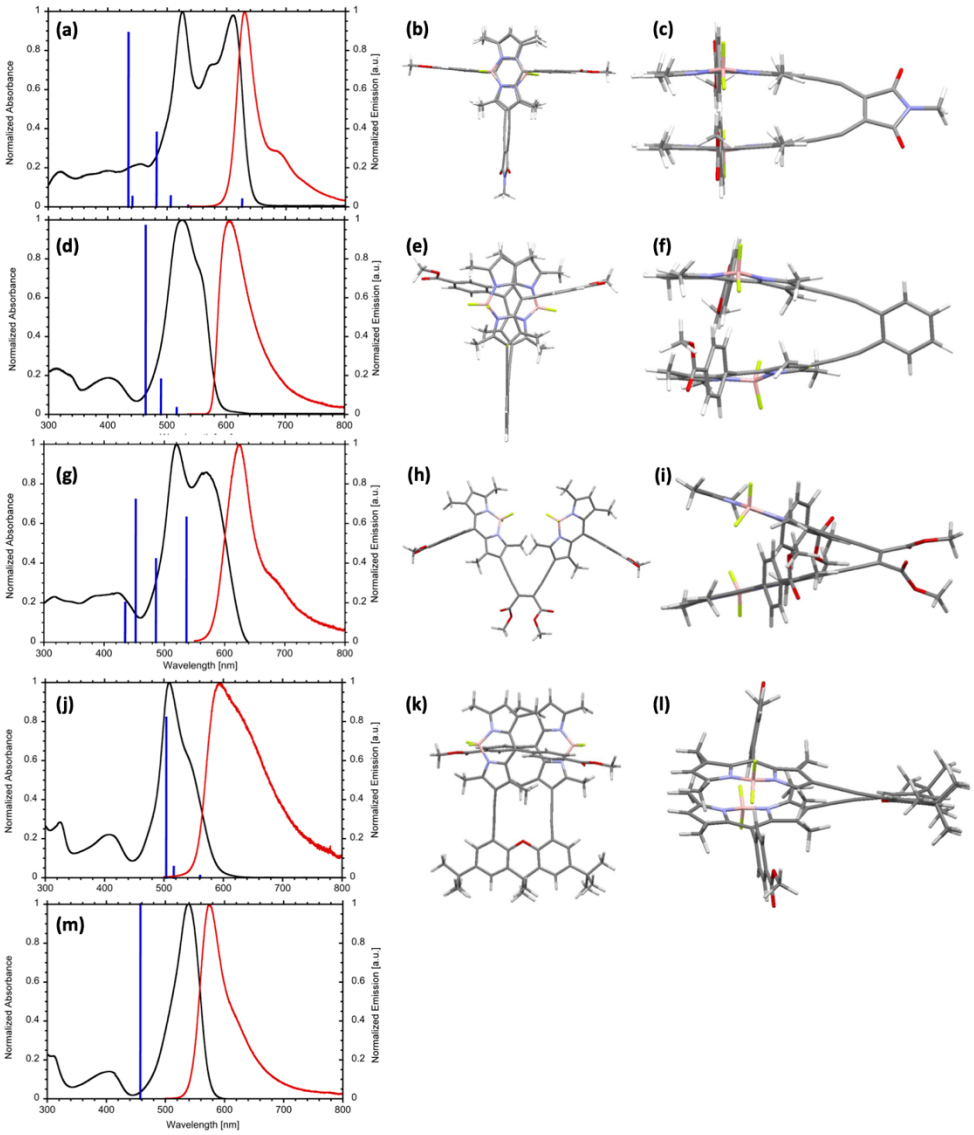

Figure 1. Spectra and structures of selected dyads. (a,d,g,j) and benchmark monomer (m). Absorption spectra (black), emission spectra (red), and calculated transitions (blue). (b,e,h,k) Side views of structures optimized in toluene using DFT with the wb97xd functional. (c,f,i,l) Top views of optimized structures. Results are shown for (a,b,c) **β-2BDP-M**, (d,e,f) ***β*-2BDP-B**, (g,h,i) ***cis*-*β*-2BDP-F**, (j,k,l) ***β*-2BDP-X** and (m) for ***β*-BDP-Ph**. For emission spectra, samples were excited at the maximum of absorption band centered at ~ 400 nm. For excitation spectra see Figure S3.

The absorption spectra for each dyad show a significant red shift as well as either splitting (for **β-2BDP-M** and ***cis*-β-2BDP-F**) or broadening of the absorption manifold localized in the visible part of the spectra, compared to the spectra of the benchmark monomer (see Table 3). The absorption spectra are essentially independent of solvent and concentration; observed features thus arise from the intermolecular interpigment interactions rather than from aggregation or other intermolecular interactions. Overall, the absorption features are consistent with significant ground-state interaction between chromophores in co-facial dyads, which leads to the formation of a series of new excited states do not present in the monomer.[53] This conclusion is also supported be the analysis of the molar extinction coefficients ε for dyads, which are not simply the sum of the ε of monomer (Table 2). The strength of interpigment excitonic interaction is defined as a half of the splitting energy between $S_0 \rightarrow S_1$ and $S_0 \rightarrow S_2$ transitions, where S_1 and S_2 are excitonic states formed upon excitonic coupling.[2,51] To quantify the strength of interpigment electronic interaction, we deconvolved the absorption spectra into separate Gaussian peaks (see Figure S4 and Table S2). Deconvolution reveals the presence of several absorption peaks in the main absorption manifold, which can be ascribed to the electronic and vibrational transitions. Unambiguous identification of 0-0 vibrational bands for $S_0 \rightarrow S_1$ and $S_0 \rightarrow S_2$ transitions is then difficult without further detailed computational analysis of vibrational features. Therefore, for evaluation of relative strength of interpigment electronic interaction we use the energy difference between the lowest- and highest-energy bands as determined by this deconvolution. The results are summarized in Table 3. Giant coupling is observed for several of the dyads, with the strongest coupling occurring for the co-facial dyad linked by the conjugated maleimide moiety **β-2BDP-M** which is manifested by a splitting of the visible absorption manifold by of 3,333 cm^{-1}.

Table 3. Optical-absorption properties of the synthesized dyads: maximum absorption wavelengths λ_{abs}, molar absorption coefficient at the maximum wavelength ϵ_{max}, transition energy difference ΔE. All data are taken in toluene.

Compound	$\boldsymbol{\lambda_{abs}}$ **[nm]**	$\boldsymbol{\epsilon_{max}}$ **[$M^{-1}\cdot cm^{-1}$]**	**ΔE [cm^{-1}]**
Co-facial arrangement, conjugated linker			
β-2BDP-M	526 576 611	41,000	3,333
β-2BDP-B	526	55,000	1,295
***cis*-β-BDP-F**	520 567	31,000	2,964
Co-facial arrangement, non-conjugated linker			
β-2BDP-X	509	75,000	2,334
Non-co-facial arrangement, conjugated linker			
***trans*-β-BDP-F**	595	–	2,861
β-2BDP-H	560	81,000	1,424
Benchmark monomer			
β-BDP-Ph	539	28,000	-

Significantly, this giant excitonic coupling is obtained while maintaining high fluorescence quantum yield and nanosecond-scale fluorescence lifetimes in toulene, as summarized in Table 4 and Figure S5. For all dyads except the one with the xanthene linker (**β-2BDP-X**), the fluorescence quantum yields are reduced by only 20% - 40% as compared to the benchmark monomer, and the emission spectra resemble that of the benchmark monomer. This indicates that emission occurs

from the lowest excitonic excited state (S_1) with nanosecond lifetimes. This observation is consistent with the previously reported femtosecond-range $S_n \rightarrow S_1$ internal conversion for excitonically coupled dyads.[81] Excitation spectra (Figure S2) are nearly identical with absorption spectra for all dyads, except ***cis*-β-2BDP-F**. The interpretation of emission data for ***cis*-β-2BDP-F** is more complex, due to the excited state *cis-trans* isomerization. However, near-identical excitation (Figure S2f) and emission spectra and Φ_f for ***cis*-β-2BDP-F** and ***trans*-β-2BDP-F** (Figure S1c) suggest that emission occurs from the same excited state for both isomers.

Comparison of the radiative rate constants, k_r, for dyads to that for monomer provides further inside into the nature of the electronic states in dyads. According to the Strickler-Berg equation, k_r is proportional to the oscillator strength of the $S_0 - S_1$ absorption band.[82] As shown in Table 4, k_r is greater for all arrays except **β-2BDP-B** than for benchmark monomer; for **β-2BDP-B**, it is approximately two times smaller than for the monomer. This is consistent with the relative intensities of the lowest-energy absorption bands obtained from deconvolution of the visible absorption manifold (see Figure S4, Table S2).

Relatively high fluorescence quantum yields and excited-state lifetimes in the nanosecond range are maintained for the co-facial dyads in polar environments, with a reduction of a factor of approximately 2 for both Φ_f and τ_f in PhCN as compared to the values in toluene. For **β-2BDP-H**, a more significant reduction is observed, by a factor of approximately 5, suggesting a contribution of the charge-transfer state to the excited state in a polar environment.[83,84]

Femtosecond transient absorption (TA) spectra together with the results of global analysis and relevant time constants are presented in Figures S6-S8. TA measurements support the interpretation of emission from the S_1 state in these dyads. TA spectra are dominated by ground-state bleaching and stimulated emission corresponding to the $S_0 - S_1$ transition. There is some dynamics in fs and ps time range observed upon global analysis, which is most likely associated with vibrational relaxation and solvent reorganization. At longer times, this bleach decays on time

scales consistent with the values of τ_f measured by time-resolved fluorescence. For **β-2BDP-M**, the bleaching signal also shows dynamics with time constants in the range of tens to hundreds of picoseconds, accompanied by a bathochromic shift (Figure S6); these dynamics are most likely caused by excited-state conformational changes that alter the interpigment electronic coupling.

Reduction of Φ_f and τ_f in PhCN compared to toluene suggests the occurrence of (possibly symmetry-breaking) electron transfer and charge separation in polar solvents. Formation of charge-separated state would be manifested by evolving of new absorbing states in TA which can be ascribed to cation-radical and/or anion-radical absorption. Analysis of the TA in polar and non-polar solvents shows no formation of such states in polar solvents. Thus, evidence for a symmetry-breaking charge separation has not been found in TA spectra for any of examined dyads in PhCN (this observation does not rule out the formation of charge-separation state, since cation/anion-radical can absorb outside the measured range).

Table 4. Optical-emission properties of the synthesized dyads: emission wavelength λ_{em}, emission linewidth (full width at half maximum, FWHM), Stokes' shift, fluorescence quantum yield Φ_f, fluorescence lifetime τ_f, radiative rate k_r, and non-radiative k_{nr} rate constants. All data are taken in toluene, except for the values for Φ_f τ_f, k_r and k_{nr} in benzonitrile (PhCN, indicated in parentheses). Stokes' shift was calculated as the difference between the longest-wavelength absorption peak as determined by the deconvolution analysis and the emission maximum. $(k_r)^{-1}$ was calculated using formula: $(k_r)^{-1} = \tau_f/\Phi_f$. $(k_{nr})^{-1}$ was calculated using formula: $(k_{nr})^{-1} = \tau_f/(\Phi_f - 1)$.

Compound	λ_{em} **[nm]**	**FWHM [cm^{-1}]**	**Stokes shift [cm^{-1}]**	Φ_f **(PhCN)**	τ_f **[ns] (PhCN)**	$(k_r)^{-1}$ **[ns] (PhCN)**	$(k_{nr})^{-1}$ **[ns] (PhCN)**
Co-facial arrangement, conjugated linker							

β-2BDP-M	631	923	465	0.48 (0.23)	2.43 ± 0.25 (1.49 ± 0.25)	5.06 (6.48)	4.67 (1.94)
β-2BDP-B	579	1228	554	0.52 (0.26)	6.11 ± 0.25 (2.79 ± 0.25)	11.75 (10.73)	12.73 (3.77)
***cis*-β-BDP-F**	624	1680	1549	0.35	–		
Co-facial arrangement, non-conjugated linker							
β-2BDP-X	592	2773	1695	0.25 (0.13)	2.65 ± 0.25 [60%] 12.6 ± 0.25 [40%] (2.03 ± 0.25 [79%] 15.3 ± 0.25 (21%])		
Non-co-facial arrangement, conjugated linker							
***trans*-β-BDP-F**	627	1089	858	0.35 (0.12)	1.03 ± .057[a] (0.416 ± 0.024)[a]	2.94 (3.47)	1.58 (0.47)
β-2BDP-H	606	1074	592	0.44 (0.08)	1.79 ± 0.25 (0.324 ± 0.023)[a]	4.07 (4.05)	3.19 (0.35)
Benchmark monomer							
β-BDP-Ph	576	1533	1090	0.61 (0.34)	4.96 ± 0.25 (3.07 ± 0.25)	8.13 (9.03)	12.72 (4.65)

[a] The excited state lifetime was obtained from fs-TA spectra.

The **β-2BDP-X** dyad is the sole exception to the observation of long-lived emission from the S_1 state. The fluorescence spectrum of this dyad is much broader than that of the other dyads,

and the fluorescence quantum yield is significantly lower than that of the benchmark monomer. Moreover, a biexponential decay is observed for this dyad, with short and long lifetimes (2.65 ns and 12.6 ns in toluene). Moreover, **β-2BDP-X** feature a substantially larger Stokes' shift and FWHM of emission spectrum, compared to other dyads and monomer. Together, these observations suggest excimer formation,[49] with the biexponential decay corresponding to emission from both the (shorter-lived) excitonic state and the (longer-lived) excimer.

Computed Electronic Structure. The spectroscopic data indicate significant excitonic coupling in the dyads, tougher with a long-lived excited state that should enable efficient energy transfer or charge extraction. The data also indicate a significant difference in the coupling strength across the various dyads. To validate the interpretation of the spectroscopic data in terms of strong interpigment electronic coupling, we calculate electronic structure and optical transition energies for the dyads with slipped co-facial arrangement of the BODIPY units.

The electronic structure of the dyads is calculated using the recently developed density functional theory framework of screened range separated hybrid functional with polarizable continuum model (SRSH-PCM).[85,86] In this framework, the frontier orbital energies are consistent with the ionization potential (IP) and electron affinity (EA) of the molecular system in the condensed phase.

Table 5. Calculated molecular-orbital energies and corresponding orbital electron densities (isodensity surfaces) for co-facial dyads in toluene, calculated using the SRSH-PCM method, with geometries optimized using the wb97xd functional. Also given are the difference in energy levels within each of the bands, Δ(HOMO) and Δ(LUMO). All energies are in eV. Calculated ionization potential and electron affinity for the monomer are 6.30 eV and 2.51 eV, respectively.

Dyad	HOMO-1	HOMO	Δ(HOMO)	LUMO	LUMO+1	Δ(LUMO)
Conjugated linkers						
β-2BDP-M (conjugated linker)	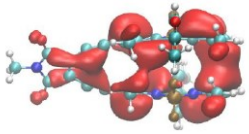 -6.42	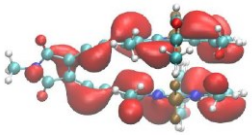 -6.04	0.38	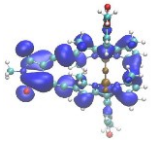 -2.96	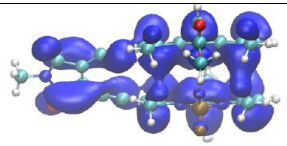 -2.69	0.27
β-2BDP-B	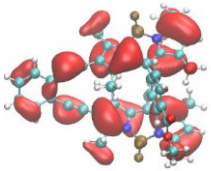 -6.28	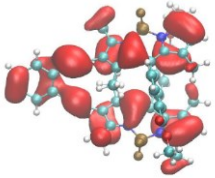 -6.09	0.19	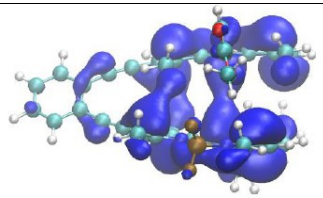 -2.75	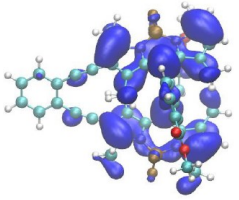 -2.67	0.08
***cis*-β-2BDP-F**	-6.23	-5.96	0.27	-2.69	-2.58	0.11
Non-conjugated linker						
β-2BDP-X	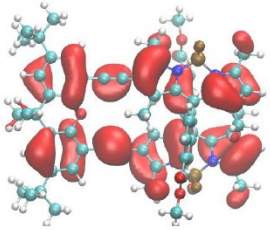 -6.07	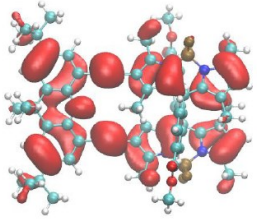 -5.82	0.25	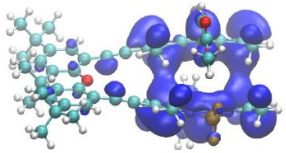 -2.72	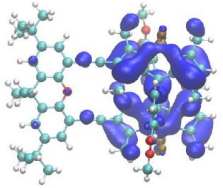 -2.56	0.16

Calculated molecular-orbital (MO) energies are given in Table 5; all values are calculated for dyads in toluene. For comparison, Table S2 lists the calculated values when the PCM model is invoked without the polarization-consistent screening framework and Table S3 lists MO calculated using the ωb97xd functional with CPCM solvatation model. In both latter cases, the MO energies remain similar to their gas-phase values, deviating from the values in solvent. The calculations show mixing of HOMO and LUMO characteristic for monomers and formation of new sets of orbitals delocalized over both BODIY subunits ("bonding" and "antibonding"). These new MOs correspond to HOMO-1 and HOMO (in case of monomer HOMO mixing) and LUMO and LUMO+1 of dyads. The energy difference within the corresponding MOs (ΔHOMO and ΔLUMO, Table 5) reflect the strength of the ground-state electronic interactions; lack of ground-state interaction would be manifested as two degenerate HOMOs and LUMOs each localized on the individual BODIPY units.[46,53,54] We note that ΔHOMO and ΔLUMO are similar when calculated using either the RSH-PCM or the SRSH-PCM model.

Also shown in Table 5 are plots of the electron distribution for the various calculated molecular orbitals. In all cases, electrons are delocalized across both coupling BODIPY subunits, again characteristic of strong ground-state interactions between the individual chromophores. Overall, then, the calculations support the interpretation of the data in terms of the formation of a new excited states due to strong inter-pigment coupling.

The order of the calculated ΔHOMO and ΔLUMO is consistent with the order of the strength of electronic interactions ΔE obtained from the absorption spectra (Table 1), providing qualitative agreement between the model and experiment. To provide further insight into the absorption properties of the dyads, we also calculate their optical transition energies. The results are given in Table 6 and plotted in Figure 1. Calculations confirmed the formation of sets of new, closely positioned excited states not observed for the monomer. We used ΔE (the difference between S_1 and S_2 calculated energies) as a measure of the strength of electronic interactions (Table 6). The

ordering of the calculated ΔE is the same as for the calculated molecular-orbital energies (ΔHOMO and ΔLUMO, Table 5) and for the experimentally measured values (see Table 3), indicating that the calculations capture the key mechanisms responsible for the modification of energy levels.

Table 6. Energies of the $S_o \rightarrow S_1$ and $S_o \rightarrow S_2$ transitions (E_{S1} and E_{S2}, respectively) and corresponding oscillator strengths (f), calculated for co-facial dyads in toluene using the SRSH-PCM method. Structures were optimized at the wb97xd level. Also shown is the calculated difference in energy levels $\Delta E = E_{S1} - E_{S2}$.

Compound	E_{S1} (eV)	f	E_{S2} (eV)	f	ΔE (cm^{-1})
Conjugated linkers					
β-2BDP-M	1.98 (626 nm) HOMO → LUMO	0.038	2.32 (534 nm) HOMO → LUMO+1	0.0066	2,709
β-2BDP-B	2.40 (517 nm) HOMO → LUMO	0.034	2.53 (490 nm) HOMO-1 → LUMO HOMO → LUMO+1	0.18	997
***cis*-β-2BDP-F**	2.31 (537 nm) HOMO → LUMO	0.63	2.55 (486 nm) HOMO → LUMO+1	0.42	1,932
Non-conjugated linker					
β-2BDP-X	2.21 (561 nm) HOMO → LUMO	0.01	2.40 (517 nm) HOMO-1 → LUMO HOMO → LUMO+1	0.056	1,531

Discussion: Mechanism of Excitonic Coupling

Experiments and calculations indicate significant variations in excitonic coupling strength among the various BODIPY dyads considered. Absorption spectra, MO calculations, and TD-DFT all indicate that the strength of the inter-BODIPY electronic interactions decreases in order **β-2BDP-M > *cis*-β-2BDP-F > β-2BDP-X** > **β-2BDP-B**.

However, the absorption and emission spectra of the arrays also significantly deviate from those predicted by Kasha's excitonic coupling model.[20,51] For example, optimized geometries for **β-2BDP-M** and **β-2BDP-X** show mutual orientation of transition dipole moments very close to

that required for H-coupling (Figure 1, Table S1); according to Kasha's model, this geometry should result in a blue shift of absorption and significant reduction of k_r. This indicates that the long-range dipole-dipole interactions considered in Kasha's model are dominated by short-range excitonic coupling due to strong ground-state inter-BODIPY interactions (through-space coupling) as well as π-conjugation provided by the conjugated linker (through-bond coupling). The similar conclusion was previously drawn for directly-linked BODIPY dyads.[53]

To distinguish between the through-space and through-bond coupling mechanisms, we perform calculations on hypothetical "disconnected" analogues of the dyads, where the ethynyl-substituted BODIY subunits are fixed in the same relative orientation and geometry as in covalent dyads, but the central part of the linker is removed and substituted by hydrogen (Tables S3-S4). Figure S9 illustrates the chemical structure of these fictional dyads. With the linker removed, there should be no through-bond coupling in these disconnected dyads; comparing the calculated coupling strengths, expressed by ΔHOMO and ΔLUMO in the connected and disconnected dyads thus gives insight into the relative contributions of through-space and through-bond coupling to the total coupling strength.

Results are tabulated in Table 7. For the maleimide- and phenyl-linked dyads, **β-2BDP-M** and **β-2BDP-B**, removing the linker has nearly no effect on the energy separations, indicating that coupling is dominated by the through-space mechanism. By contrast, removing the linker substantially reduces the energy separation for the maleate- and xanthene-linked dyads, **β-2BDP-F** and **β-2BDP-X**, but with significant separation remaining in the disconnected dyads; this indicates contributions from both through-space and through-bound coupling.

Table 7. Calculated difference between energy levels within the MOs ΔHOMO and ΔLUMO, and calculated difference between peaks in the optical absorption spectrum, ΔE, for co-facial dyads in toluene. Values are calculated using the real structure of the dyads (Real) and using fictional "disconnected" structures where the linker was removed (Dis). Also shown are the computed center-to-center (R_{CC}) and edge-to-edge (R_{EE}) distances are given. R_{CC} is defined as the shortest carbon to carbon distance across the two units.

Dyad	ΔHOMO (eV)		ΔLUMO (eV)		ΔE (cm^{-1})		R_{CC} (Å)	R_{EE} (Å)
	Real	**Dis**	**Real**	**Dis**	**Real**	**Dis**		
Conjugated linkers								
β-2BDP-M	0.38	0.38	0.27	0.27	2,709	2,500	4.00	3.54
β-2BDP-B	0.19	0.17	0.08	0.06	997	887	5.70	4.08
***cis*-β-2BDP-F**	0.27	0.04	0.11	0.04	1,932	806	5.06	3.88
Non-conjugated linker								
β-2BDP-X	0.25	0.13	0.16	0.16	1,531	887	8.10	4.40

Analysis of electronic and structural factors provides a rationale for these findings (see Table 7 and Figure 1). For **β-2BDP-M**, the relatively short center-to-center distance and slipped-co-facial arrangement results in strong through-space electronic interaction. On the other hand, significant twisting of the BODIPY plane *versus* the enediyne linker plane (~ 48°) prevents substantial through-bond π-conjugation, despite the conjugated linker. Similar twisting of BODIPY *versus* the 1,2-diethynylbenzen linker prevents π-conjugation in **β-2BDP-B**; in this case, a larger inter-BODIPY distance results in a weaker through-space coupling. For ***cis*-β-2BDP-F**, the edge-to-edge and center-to-center distances are even larger and the BODIPY subunits have a large lateral displacement relative to one another, leading to weak through-space interactions. On the other hand, the dihedral angle between the BODIPY plane and C=C bond of the linker is relatively small (~30°), enabling through-bond π-conjugation. **β-2BDP-X** exhibits significant through-bond coupling, even in the absence of a π-conjugated linker. The xanthene linker can be considered formally as a homoconjugated moiety, since one sp^3 carbon intervenes conjugated aromatic rings.[87] Excitonic delocalization mediated by a saturated bridge has also been reported.[88-

[91] In addition, the dihedral angle between xanthene and the BODIPY planes is relatively small (~25°), facilitating through-bond coupling.

Overall, for the BODIPY dyads studied, there is a tradeoff between maximizing through-space coupling, by minimizing inter-pigment separation, and maximizing through-bond coupling, by minimizing distortion of the bond angle in the linking moiety. The largest coupling strength is obtained by almost entirely sacrificing through-bond coupling in order to bring the BODIPY units as close as possible to one another. Future work will be dedicated to further increasing coupling strength by developing molecular arrays with linking units that allow both small interpigment distances and strong through-bond π-conjugation.

Conclusions.

Arranging BODIPY into arrays with strong interpigment interactions leads to chromophores with giant excitonic coupling and broad absorbance. Comparing BODIPY dyads with different linking units allowed us to determine the mechanisms responsible for the interactions and the design rules to engineer giant excitonic interaction between the BODIPY subunits. Dyads with slipped co-facial alignment of the BODIPY subunits exhibited strong coupling and significant fluorescence in both polar and non-polar solvents. Both through-bond and through-space interactions can contribute to excitonic coupling; however, the largest coupling was observed in the cases when through-space interactions were minor. This arose because maximizing through-space interactions requires minimizing interpigment distance, which in turn reduced through-bond π-conjugation due to inferred geometrical strain.

We also observed that a non-conjugated xanthene linker can lead to significant through-bond coupling, confirming earlier findings.[88,90,91] In this case, interpretation of the optical spectra is complicated by possible excimer formation. Interpretation of the data is complicated in the case of diethynylmaleate-linked dyads by *cis-trans* photoisomerization, which also complicates its

potential applications. By contrast, other dyads, notably those with maleimide linkers, exhibited giant coupling, broad absorption, photostability, and relatively long excited-state lifetime in non-polar and moderately polar environments, making them promising materials for solar energy conversion and other photonic applications.

Experimental Section.

Photophysical measurements. Absorption spectra were taken at room tempertature. Static emission spectra were taken in air-equilibrated solvent at room temperature in dilluted solution, with absorbance below 0.1. Quantum yields were determined in air-equilibrated solvents using Rhodamine 6G in air-equilibrated MeOH ($\Phi_f = 0.88$) or tetraphenylporphyrin in air-equilibrated toluene ($\Phi_f = 0.070$)[92] as a standard.

Transient absorption (TA) measurements are performed using a Helios spectrometer (Ultrafast Systems). Pump and probe laser pulses are derived from a regeneratively amplified Ti:Sapphire oscillator (Spectra Physics Tsunami/SpitfirePro) operating at 2 kHz. The pump pulse is passed to an optical parametric amplifier (OPA; Light Conversion TOPAS/NIRuVis) which is then selected to a have a wavelength corresponding to the specified absorption band of the array. The samples are prepared by dissolving the dyads in toluene or PhCN such that the absorption bands being monitored have an optical density (OD) between 0.3 and 0.6. The prepared samples are placed in a 2mm quartz cuvette which is housed in a thermoelectric temperature-controlled sample holder and all measurements are performed at 20°C. The sample is continuously stirred over the duration of the measurements to eliminate any thermal artifacts from the pump laser pulse. Pump laser pulse energies are set between 0.8μJ and 1.0μJ for all TA measurements. Analysis and fitting of the TA measurements is done using SurfaceXplorer (Ultrafast Systems); errors in the

reported lifetimes correspond to errors obtained from the fits of the TA kinetics. The temporal resolution of instrument is 150 fs.

Time resolved photoluminescence (PL) measurements are performed by time-correlated single-photon counting (TCSPC). The samples are excited using a 510 nm pulsed diode laser (PicoQuant PDL 800-D) with a pulse width of approximately 150 nm. Individual photons are detected by an avalanche photodiode (MPD PDM Series) and the timing of the detected photon, referenced to the corresponding excitation pulse, are synchronized using timing electronics (PicoQuant PicoHarp 300). A histogram of the counts is then compiled over time and a least-squares fitting routine is performed to determine the lifetimes. Errors in the reported lifetimes correspond to the instrument response function (IRF).

Computation. Screened range separated hybrid (SRSH) functional based on the LRC-wPBEh functional in combination with polarizable continuum model (PCM) was employed to determine orbital energies and excitation energies in toluene medium. For comparison, B3LYP, wB97X-D, and the corresponding unscreened functional energies all within PCM are provided as well. In establishing the SRSH framework, a generalized Kohn-Sham formulation is invoked, where the functional is expressed as follows:

$$E_{XC}^{SRSH} = \alpha E_{Fx}^{SR} + (1-\alpha)E_{DFx}^{SR} + (\alpha+\beta)E_{Fx}^{LR} + (1-\alpha-\beta)E_{DFx}^{LR} + E_{DFc} .$$

Here, the subscripts X and C stand for exchange and correlation, the subscripts F and DF represent exact and the chosen semilocal exchange functional. The SR and LR labels stand for short-range and long-range terms, respectively. In SRSH-PCM calculations, the LR weight is reset to the scalar dielectric constant of the solvent, $\alpha + \beta = 1/\epsilon$, where α is fixed at a default value (as widely used, $\alpha = 0.2$). The range-separation parameter is tuned by relating the HOMO energies of the neutral and of the anion to the corresponding ionization potential, where the range separation tuning is performed in the gas phase without PCM. Absorption energies are calculated using the ground state optimized geometry in toluene, which is obtained by using the dispersion corrected wB97X-

D functional, invoking solvent effect by the PCM approach. All the calculations (unless noted otherwise) are performed in Q-Chem 4.4 using 6-31++G(d,p) basis set.

Synthesis and characterization. ^{1}H NMR spectra (400 MHz) and ^{13}C NMR (100 MHz) spectra were collected at room temperature in $CDCl_3$. Chemical shifts (δ) were calibrated using residual solvent peaks (proton signals: 7.26 ppm for chloroform, 2.50 for DMSO, ^{13}C signals: 77.0 for chloroform, 39.5 ppm for DMSO). All solvents and commercialy available reagents were used as received.

General Procedure for Palladium Catalyzed Cross-Coupling Reactions. For all Sonogashira coupling reactions, all solvents and reagents except catalyst and highly volatile liquids (such as trimethylsilylacetylene or phenylacetylene) were placed into a dried Schlenk flask then degassed by three cycles of freeze-pump-thaw. While under positive pressure of N_2, catalyst was added to the flask, and subjected to a fourth and final cycle of freeze-pump-thaw. If necessary, volatile liquids were added in during the final cycle. The exterior of flask was then cleaned of any ice that formed during degassing and placed in an oil bath at the designated temperature.

The known compound **BDP-1** was prepared following the reported procedure.[76]

β-BDP-I. Samples of **BDP-1** (60 mg, 0.157 mmol) and I_2 (19.9 mg, 0.078 mmol) were dissolved in CH_2Cl_2 (13 mL) and ethanol (26 mL). In a separate flask, iodic acid (HIO_3, 13.8 mg, 0.078 mmol) was dissolved in water (13 mL). The solution of iodic acid was slowly transferred to the second flask containing the **BDP-1**/I_2 mixture. The resulting mixture was heated at 50 °C for one hour. The reaction was monitored via TLC and starting **BDP-1** was consumed in ~ 1h. The mixture was diluted with CH_2Cl_2, washed (water and brine), dried (Na_2SO_4), and concentrated. Column chromatography [silica, hexanes/CH_2Cl_2 (1:1), second band (pink)] provided an orange-red solid (51.3 mg, 77% yield.) ^{1}H NMR (400 MHz, $CDCl_3$): δ 1.36 (s, 6H), 2.57 (s, 3H), 2.64 (s, 3H), 3.98 (s, 3H), 6.05 (s, 1H), 7.39 (d, J = 7.3 Hz, 2H), 8.20 (d, J = 7.3 Hz, 2H); ^{13}C{^{1}H} NMR (125 MHz, $CDCl_3$): δ 14.8, 14.9, 16.0, 16.9, 46.9, 52.6, 112.7, 128.4, 130.6, 131.2, 131.5, 139.7,

140.1, 143.1, 144.9, 154.7, 155.2, 158.4, 166.5; HRMS (APCI-TOF) *m/z* Calcd for $[M+H]^+$ $C_{21}H_{20}BF_2IN_2O_2$, 509.0707; Found 509.0688.

***β-BDP-TMS*.** Following the general procedure for Sonogashira reaction, a solution of ***β*-BDP-I** (30 mg, 0.059 mmol), trimethylsilylacetylene (23.2 mg, 0.236 mmol), $Pd(PPh_3)_2Cl_2$ (6.2 mg, 0.009 mmol), and CuI (1.7 mg, 0.009 mmol) in THF/Et_3N (10 mL) was heated at 50 °C for 24 hours, protected from light. After 24 hours, the reaction mixture was diluted with ethyl acetate, washed (water and brine), dried (Na_2SO_4), and concentrated. Column chromatography [silica, hexanes/ethyl acetate (3:1), second band (orange)] provided an orange-red solid (41.9 mg, 85% yield.) ^{1}H NMR (400 MHz, $CDCl_3$): δ 0.20 (s, 9H), 1.37 (s, 3H), 1.41 (s, 3H), 2.57 (s, 3H), 2.63 (s, 3H), 3.98 (s, 3H), 6.03 (s, 1H), 7.38 (d, J = 8.3 Hz, 2H), 8.19 (d, J = 8.3 Hz, 2H); ^{13}C{^{1}H} NMR (125 MHz, $CDCl_3$): δ 0.45, 13.6, 13.8, 15.0, 15.1, 52.7, 97.6, 101.6, 122.7, 128.6, 129.8, 130.8, 131.3, 132.3, 139.8, 140.9, 143.4, 144.7, 157.7, 158.5, 166.7; HRMS (APCI-TOF) *m/z* Calcd for $[M+H]^+$ $C_{26}H_{29}BF_2N_2O_2Si$, 479.2137; Found 479.2133.

β-BDP-EH. A sample of ***β*-BDP-TMS** (41.9 mg, 0.088 mmol) and potassium carbonate (13.3 mg, 0.096 mmol) in THF/MeOH ((1:1), (10 mL)) was stirred at room temperature for one hour. The reaction mixture was diluted in CH_2Cl_2, washed (water and brine), dried (Na_2SO_4), and concentrated. Column chromatography [silica, hexanes/CH_2Cl_2 (1:1), third band (orange)] provided a red solid (29.6 mg, 83% yield). ^{1}H NMR (500 MHz, $CDCl_3$): δ 1.37 (s, 3H), 1.42 (s, 3H), 2.57 (s, 3H), 2.63 (s, 3H), 3.29 (s, 1H), 3.97 (s, 3H), 6.04 (s, 1H), 7.39 (d, J = 7.9 Hz, 2H), 8.19 (d, J = 7.9 Hz, 2H); ^{13}C{^{1}H} NMR (125 MHz, $CDCl_3$): δ 13.2, 13.4, 14.7, 14.9, 29.7, 52.5, 76.2, 83.7, 114.3, 122.6, 128.3, 129.4, 130.5, 131.1, 132.1, 139.4, 140.8, 143.4, 144.8, 157.1, 158.7, 166.4; HRMS (APCI-TOF) *m/z* Calcd for $[M+H]^+$ $C_{23}H_{21}BF_2N_2O_2$, 407.1741; Found 407.1736.

β-BDP-Ph. Following the general procedure for Sonogashira reaction, a solution of **β-BDP-I** (16.0 mg, 0.031 mmol), phenylacetylene (12.9 mg, 0.126 mmol), $Pd(PPh_3)_4$ (5.5 mg, 0.005

mmol), and CuI (0.90 mg, 0.005 mmol) in THF/Et_3N (1:1) (6 mL) was stirred at 50 °C for 24 hours protected from light. The reaction mixture was diluted with ethyl acetate, washed (water and brine), dried (Na_2SO_4), and concentrated. Column chromatography [silica, CH_2Cl_2/hexanes (1:1), second band (pink, orange fluorescence)] provided a pink film (11.6 mg, 76% yield.) ^{1}H NMR (400 MHz, $CDCl_3$): δ 1.37 (s, 3H), 1.48 (s, 3H), 2.58 (s, 3H), 2.70 (s, 3H), 3.97 (s, 3H), 6.03 (s, 1H), 7.29 – 7.31 (m, 2H), 7.41 (d, J = 8.5 Hz, 2H), 7.43 – 7.45 (m, 2H), 8.20 (d, J = 8.0 Hz, 2H); $^{13}C\{^1H\}$ NMR (125 MHz, $CDCl_3$): δ 13.2, 13.5, 14.6, 14.7, 29.6, 52.4, 81.6, 96.0, 115.4, 122.3, 123.3, 127.9, 128.2, 129.7, 130.4, 130.9, 131.2, 131.8, 139.4, 140.4, 142.3, 144.2, 157.0, 158.0, 166.3; HRMS (MALDI-FTICR) *m/z* Calcd for $[M]^+$ $C_{29}H_{25}BF_2N_2O_2$, 482.1977; Found 482.1972.

β-2BDP-M. Following the general procedure for Sonogashira reaction, a solution of ***β*-BDP-EH** (16.5 mg, 0.041 mmol), *N*-methyl-2,3-dibromomalemide **1** (5.42 mg, 0.020 mmol), $Pd_2(dba)_2$ (5.58 mg, 0.006 mmol) and P(o-tol)$_3$ (5.56 mg, 0.018) in toluene/Et_3N (5:1, 6 mL) was stirred at 60 °C for 24 hours protected from light. The mixture was diluted in ethyl acetate, washed (water and brine), dried (Na_2SO_4) and concentrated. Column chromatography [silica, hexanes/CH_2Cl_2/ethyl acetate (3:10:1), third band (purple, dark red fluorescence)] provided a blue-purple solid. There is a pink impurity that does not initially appear on TLC but appears to coelute with the product. Wash with methanol and filer to obtain pure product (8.5 mg, 45% yield.) ^{1}H NMR (400 MHz, $CDCl_3$): δ 1.42 (s, 6H), 1.51 (s, 6H), 2.63 (s, 3H), 2.61 (s, 6H), 2.68 (s, 6H), 3.06 (s, 3H), 4.02 (s, 6H), 6.13 (s, 2H), 7.42 (d, J = 7.5 Hz, 4H), 8.24 (d, J = 7.5 Hz, 4H); $^{13}C\{^1H\}$ NMR (125 MHz, $CDCl_3$): δ 13.3, 14.8, 52.5, 88.7, 103.2, 113.8, 123.5, 124.5, 128.2, 129.7, 130.7, 131.3, 133.0, 138.9, 141.0, 142.6, 143.2, 145.9, 157.1, 160.5, 166.3, 167.6; HRMS (ESI-FTICR) *m/z* Calcd for $[M+H]^+$ $C_{51}H_{43}B_2F_4N_5O_6$, 920.3425; Found 920.3429.

β-2BDP-B. Following the general procedure for Sonogashira reaction, a mixture of ***β*-BDP-EH** (15.0 mg, 0.037 mmol), 1,2-dibromobenzene **2** (4.36 mg, 0.018 mmol), $Pd_2(dba)_3$ (5.1 mg, 0.006 mmol) and P(o-tol)$_3$ (5.1 mg, 0.017 mmol) in toluene/Et_3N (5:1) (6 mL) was stirred at

60 °C for 24 hours protected from light. The mixture was diluted with ethyl acetate, washed (water and brine), dried (Na_2SO_4) and concentrated. Gravity column chromatography [silica, CH_2Cl_2, second band (pink, orange fluorescence)] provided a red film (10.0 mg, 61% yield.) ^{1}H NMR (400 MHz, $(CD_3)_2CO$): δ 1.43(s, 6H), 1.45 (s, 6H), 2.57 (s, 12H), 4.00 (s, 6H), 6.28 (s, 2H), 7.37 (ddd, *J* = 1.3, 3.3, 5.8 Hz, 2H), 7.55 (ddd, *J* = 1.3, 3.4, 5.7 Hz, 2H), 7.61 (dd, *J* = 1.3, 8.4 Hz, 4H), 8.22 (dd, *J* = 1.3, 8.4 Hz, 4H); $^{13}C\{^1H\}$ NMR (125 MHz, $CDCl_3$): δ 13.4, 13.6, 14.7, 14.9, 52.4, 85.9, 94.9, 115.4, 122.4, 125.5, 127.8, 128.3, 129.7, 130.5, 131.0, 131.8, 132.1, 139.5, 140.6, 142.3, 144.5, 157.1, 158.3, 166.4. HRMS (ESI-FTICR) *m/z* Calcd for $[M+Na]^+$ $C_{52}H_{44}B_2F_4N_4O_4$, 909.3393; Found 909.3397.

β-2BDP-H was isolated as a side product in non-optimized synthesis of **β-2BDP-B**. Following the general procedure for Sonogashira reaction, a mixture of **β-BDP-EH** (30 mg, 0.0739 mmol), 1,2-dibromobenzene **2** (8.7 mg, 0.0369 mmol), $Pd(PPh_3)_2Cl_2$ (15.5 mg, 0.0222 mmol), CuI (4.22 mg, 0.0222 mmol), and triethylamine (7.47 mg, 0.0739 mmol) in THF (10 mL) was stirred at 50 °C for 24 hours protected from light. The mixture was diluted in ethyl acetate, washed (water and brine), dried (Na_2SO_4) and concentrated. Gravity column chromatography [silica, CH_2Cl_2, first band (purple, red fluorescence)] provided a purple film (22.8 mg, 76% yield.). ^{1}H NMR (500 MHz, $CDCl_3$): δ 1.37 (s, 6H), 1.42 (s, 6H), 2.57 (s, 6H), 2.65 (s, 6H), 3.98 (s, 6H), 6.06 (s, 2H), 7.38 (d, *J* = 8.1 Hz, 4H), 8.19 (d, *J* = 8.1 Hz, 4H); $^{13}C\{^1H\}$ NMR (125 MHz, $CDCl_3$): δ 13.4, 13.8, 14.8, 14.9, 52.6, 75.5, 80.3, 114.1, 122.9, 128.3, 129.4, 13.6, 131.2, 132.5, 139.3, 140.8, 143.7, 145.2, 158.1, 159.3, 166.5. HRMS (ESI-FTICR) *m/z* Calcd for $[M+H]^+$ $C_{46}H_{40}B_2F_4N_4O_4$, 811.3259; Found 811.3239.

trans-β-2BDP-F. Samples of **β-BDP-EH** (15.0 mg, 0.037 mmol), dimethyl *trans*-2,3-bromobutenedioate **3** (5.57 mg, 0.018 mmol), $Pd(PPh_3)_2Cl_2$ (2.54 mg, 0.003 mmol) and $P(o\text{-}tol)_3$ (2.53 mg, 0.008 mmol) in toluene/Et_3N (5:1, 6 mL) were heated to 60ºC for 20 hours protected from light. The mixture was diluted in ethyl acetate, washed (water and brine), dried (Na_2SO_4) and

concentrated. Column chromatography [silica, CH_2Cl_2, protected from light, fourth band (purple)] provided a purple-blue solid (10.7 mg, 61% yield.) ^{1}H NMR (400 MHz, $CDCl_3$): δ 1.39 (s, 6H), 1.47 (s, 6H), 2.59 (s, 6H), 2.67 (s, 6H), 3.79 (s, 6H), 3.98 (s, 6H), 6.07 (s, 2H), 7.31 (dd, *J* = 4.0, 8.1 Hz, 4H), 8.20 (dd, *J* = 4.0, 8.5 Hz, 4H); HRMS (ESI-FTICR) *m/z* Calcd for $[M+H]^+$ $C_{52}H_{46}B_2F_4N_4O_2$, 953.3527; Found 953.3531.

cis-β-2BDP-F. A solution of ***trans*-β-2BDP-F** in toluene with an absorbance of ~1.0 was irradiated in the 3 mL quartz cuvette in the fluorimeter measuring chamber with monochromatic light with λ = 594 nm (xenon lamp, slit width 10 nm) in 10 second intervals. The solution was stirred continuously. The absorbance spectrum was recorded after each interval. The sample was irradiated until the photostationary state was achieved (~3 minutes).

β-2BDP-X. Following the general procedure for Sonogashira reaction, a mixture of **β-BDP-EH** (15.0 mg, 0.037 mmol), 4,5-dibromo-2,7-bis(1,1-dimethylethyl)-9,9-dimethyl-9H-xanthene **4** (8.87 mg, 0.018 mmol), $Pd_2(dba)_3$ (2.54 mg, 0.003 mmol) and $P(o\text{-}tol)_3$ (2.53 mg, 0.008 mmol) in toluene/Et_3N (5:1) (6 mL) was heated to 60 °C for 23 hours protected from light. The reaction mixture was diluted with ethyl acetate, washed (water and brine), dried (Na_2SO_4), and concentrated. Gravity column chromatography [silica, CH_2Cl_2, third band (pink-purple, pink fluorescence)] provided a dark pink film (15.6 mg, 75 % yield.) ^{1}H NMR (400 MHz, ($CDCl_3$): δ 1.29 (s, 18H), 1.33 (s, 6H), 1.47 (s, 6H), 1.62 (s, 6H), 2.41 (s, 6H), 2.49 (s, 6H), 3.98 (s, 6H), 5.88 (s, 2H), 7.30 (d, *J* = 2.6 Hz, 2H), 7.34 (d, *J* = 2.5 Hz, 2H), 7.39 (d, *J* = 8.4 Hz, 4H), 8.17 (d, *J* = 8.5 Hz, 4H); $^{13}C\{^1H\}$ NMR (126 MHz, $CDCl_3$): δ 13.2, 13.4, 14.5, 14.6, 31.4, 32.5, 34.4, 34.6, 52.4, 85.6, 92.3, 111.2, 116.0, 121.5, 123.2, 128.3, 128.4, 129.4, 130.5, 130.8, 131.8, 139.8, 141.0, 142.8, 143.2, 145.4, 148.3, 156.4, 157.6, 166.7; HRMS (MALDI-FTICR) *m/z* Calcd for $[M]^+$ $C_{69}H_{68}B_2F_4N_4O_5$, 1130.5327; Found 1130.5296.

Acknowledgements.

M. Ptaszek acknowledges financial support by the National Science Foundation (grant CHE-1955318). M. Pelton and M. Ptaszek acknowledge financial support by UMBC (START Award). B.D. Dunietz acknowledges financial support by U.S. Department of Energy, Office of Basic Energy Sciences (award number DE-SC0016501). We are thankful to the Ohio Supercomputer Center[93] and the Kent State University College of Arts and Sciences making the computing facilities available to complete the reported research.

Associated Content

Additional spectral data, deconvolution of absorption spectra, time-resolved fluorescence, transient-absorption spectra, additional computational results. This material is available free of charge via the Internet at http://pubs.acs.org.

Corresponding Authors

mptaszek@umbc.edu (M. Ptaszek)
mpelton@umbc.edu (M. Pelton)
bdunietz@kent.edu (B.D. Dunietz)

References.

(1) Blankenship, R. E. *Molecular Mechanisms of Photosynthesis*; John Wiley & Sons, 2014.

(2) Mirkovic, T.; Ostroumov, E. E.; Anna, J. M.; van Grondelle, R.; Govindjee, Scholes, G. D. Light Absorption and Energy Transfer in the Antenna Complexes of Photosynthetic Organisms. *Chem. Rev.* **2017**, *117*, 249-293.

(3) Scholes, G. D.; Fleming, G. R.; Olaya-Castro, A.; van Grondelle, R. Lessons from Nature About Solar Light Harvesting. *Nature Chemistry*, **2011**, *3*, 763-774.

(4) Kálmán, L.; Williams, J. C.; Allen, J. P. Comparison of Bacterial Reaction Centers and Photosystem II. *Photosynth. Res.* **2008**, *98*, 643-655.

(5) van Amerongen, H.; Valkunas, L.; van Grondelle, R. Photosynthetic Excitons. World Scientific, New Jersey, 2000.

(6) Scholes, G. D.; Fleming, G. R.; Chen, L. X.; Aspuru-Guzik, A.; Buchleitner, A.; Coker, D. F.; Engel, G. S.; van Grondelle, R.; Ishizaki, A.; Jonas, D. M.; Lundeen, J. S.; McCusker, J. K.; Mukamel, S.; Ogilvie, J. F.; Olaya-Castro, A.; Ratner, M. A.; Spano, F. C.; Whaley, K. B.; Zhu, X. Using Coherence to Enhance Function in Chemical and Biophysical Systems. *Nature*, **2017**, *543*, 647-656.

(7) Romero, E.; Novoderezhkin, V.; van Grondelle, R. Quantum Design of Photosynthesis for Bio-Inspaired Solar-Energy Conversion. *Nature*, **2017**, *543*, 355-365.

(8) Ma, F.; Romero, El.; Jones, M. R.; Novoderezhkin, V. I.; van Grondelle, R. Vibronic Coherence in the Charge Separation Process of the *Rhodobacter Spheroides* Reaction Center. *J. Phys. Chem. Lett.* **2018**, *9*, 1827-1832.

(9) Fuller, F. D.; Pan, J.; Gelzinis, A.; Butkus, V.; Senlik, S. S.; Wilcox, D. E.; Yocum, C. F.; Valkunas, L.; Abramavicius, D.; Ogilvie, J. F. Vibronic Coherence in Oxygenic Photosynthesis. *Nat. Chem.* **2014**, *6*, 706-711.

(10) Romero, E.; Augulis, R.; Novoderezhkin, V. I.; Ferretti, M.; Thieme, J.; Zigmantas, D.; van Grondelle, R. Quantum Coherence in Photosynthesis for Efficient Solar-Energy Conversion. *Nature Phys.* **2014**, *10*, 676-682.

(11) Duan, H.-G.; Prokhorenko, V. I.; Cogdell, R. J.; Ashraf, K.; Stevens, A. L.; Thorwart, M.; Miller, R. J. D. Nature does nor Rely on Long-Lived Electronic Quantum Coherence for Photosynthetic Energy Transfer. *Proc. Natl. Acad. Sci. US.A.* **2017**, *114*, 8493-8498.

(12) Lee, H.; Cheng, Y.-C.; Fleming, G. R. Coherence Dynamics in Photosynthesis: Protein Protection of Excitonic Coherence. *Science*, **2007**, *316*, 1462-1465.

(13) Fujihashi, Y.; Higashi, M.; Ishizaki, A. Intramolecular Vibrations Complement the Robustness of Primary Charge Separation in a Dimer Model of the Photosystem II Reaction Center. *J. Phys. Chem. Lett.* **2018**, *9*, 4921-4929.

(14) Novoderezhkin, V. I.; Romero, E.; van Grondelle, R. How Exciton-vibrational Coherences Control Charge Separation in the Photosystem II Reaction Center. *Phys. Chem. Chem. Phys.* **2015**, *17*, 30828-30841.

(15) Ferretti, M.; Novoderezhkin, V. I.; Romero, E.; Augulis, R.; Pandit, A.; Zigmantas, D.; van Grondelle, R. The Nature of Coherence in the B820 Bacteriochlorophyll Dimer Revealed by Two-Dimensional Electronic Spectroscopy. *Phys. Chem. Chem. Phys.* **2014**, *16*, 9930-9939.

(16) Novoderezhkin, V. I.; Romero, E.; Prior, J.; van Grondelle, R. Exciton-Vibrational Resonance and Dynamics of Charge Separation in the Photosystem II Reaction Center. *Phys. Chem. Chem. Phys.* **2017**, *19*, 5195-5208.

(17) Novoderezhkin, V. I.; V. I.; Romero, E.; van Grondelle, R. How Excitonic-Vibrational Coherence Control Charge Separation in the Photosystem II Reaction Center. *Phys. Chem. Chem. Phys.* **2015**, *17*, 30829-30841.

(18) Ma, F.; Romero, E.; Jones, M. R.; Novoderezhkin, V. I.; van Grondelle, R. Both Electronic and Vibrational Coherences are Involved in Primary Electron Transfer in Bacterial Reaction Center. *Nat. Comm.* **2019**, *10*, Article Number 933.

(19) Policht, V. R.; Niedringhaus, A.; Willow, R.; Laible, P. D.; Bocian, D. F.; Kirmaier, C.; Holten, D.; Mancal, T.; Ogilvie, J. P. Hidden Vibronic and Excitonic Structure and Vibronic Coherence Transfer in the Bacterial Reaction Center. *Sci. Adv.* **2022**, *8*, aebk0953.

(20) Hestand, N. J.; Spano, F. C. Expanded Theory of H- and J-Molecular Aggregates: The Effect of Vibronic Coupling and Intermolecular Charge Transfer. *Chem. Rev.* **2018***, 118*, 7069-7163.

(21) Hestand, N. J.; Spano, F. C. Molecular Aggregate Photophysics Beyond the Kasha Model. Novel Design Principles for Organic Material. *Acc. Chem. Res.* **2017**, *50*, 341-350.

(22) Wasielewski, M. R. Self-Assembly Strategies for Integrating Light Harvesting and Charge Separation in Artificial Photosynthetic Systems. *Acc. Chem. Res.* **2009**, *42*, 1910-1921.

(23) Kim, D.; Osuka, A. Directly Linked Porphyrin Arrays with Tunable Excitonic Interactions. *Acc. Chem. Res.* **2004**, *37*, 735-745.

(24) Tanaka, T.; Osuka, A. Conjugated Porphyrin Arrays: Synthesis, Properties, and Application for Functional Materials. *Chem. Soc. Rev.* **2014**, *44*, 943-969.

(25) Wurthner, F.; Saha-Moller, C.; Fimmel, B.; Ogi, S.; Leowanawat, P.; Schmidt, D. Perylene Bisimide Dye Assemblies as Archetype Functional Supramolecular Materials. *Chem. Rev.* **2016**, *116*, 962-1052.

(26) Bialas, D.; Kirchner, E.; Rohr, M. I. S.; Wurthner, F. Perspective in Dye Chemistry: A Rational Approach toward Functional Materials by Understanding the Aggregate State. *J. Am. Chem. Soc.* **2021**, *143*, 4500-4518.

(27) Yang, S.-Y.; Qu, Y.-K.; Liao, L.-S.; Jiang, Z.-Q.; Lee, S.-T. Research Progress of Intramolecular π-Stacked Small Molecules for Device Applications. *Adv. Mater.* **2021**, 2104125-1-25.

(28) Madhu, M.; Ramakrishnan, R.; Vijay, V.; Hariharan, M. Free Charge Carriers in Homo-Sorted π-Stacks of Donor-Acceptor Conjugates. *Chem. Rev.* **2021**, *121*, 8234-8284.

(29) Johnson, J. C.; Nozik, A. J.; Michl, J. The Role of Chromophore Coupling in Singlet Fission. *Acc. Chem. Res.* **2013**, *46*, 1290-1299.

(30) Saal, F.; Zhang, F.; Holzapfel, M.; Stolte, M.; Michail, E.; Moos, M.; Schmeidel, A.; Krause, A.-M.; Lambert, C.; Wurthner, F.; Ravat, P. [n]Helicene Diimides (n = 5, 6, and 7): Through-Bond versus Through-Space Conjugation. *J. Am. Chem. Soc.* **2020**, *142*, 21298-21303.

(31) Peters, G. M.; Grover, G.; Maust, R. L.; Colwell, C. E.; Bates, H.; Edgell, W. A.; Jasti, R.; Kertesz, M.; Tovar, J. D. Linear and Radial Conjugation in Extended π-Electron Systems. *J. Am. Chem. Soc.* **2020**, *142*, 11431-11439.

(32) Tykwinski, R. R. Synthesis of Unsymmetrical Derivatives of Pentacene for Materials Applications. *Acc. Chem. Res*. **2019**, *52*, 2056-2069.

(33) Patalog, L. J.; Ho, L. P.; Jones, P. G.; Werz, D. B. Ethene-Bridged Oligo-BODIPYs: Access to Intramolecular J-Aggregates and Superfluorophores. *J. Am. Chem. Soc.* **2017**, *139*, 15104-15113.

(34) Lambert, C.; Scherpf, T.; Ceymann, H.; Schmeidel, A.; Holzapfel, M. Coupled Oscillators for Tuning Properties of Squaraine Dyes. *J. Am. Chem. Soc.* **2015**, *127*, 3547-3557.

(35) Korovina, N. V.; Joy, J.; Feng, X.; Feltenberger, C.; Krylov, A. I.; Bradforth, S. E.; Thompson, M. E. Linker-Dependent Singlet Fission in Tetracene Dimers. *J. Am. Chem. Soc.* **2018**, *140*, 10179-10190.

(36) Korovina, N. V.; Das, S.; Nett, Z.; Feng, X.; Joy, J.; Haiges, R.; Krylov, A. I.; Bradforth, S. E.; Thompson, M. E. Singlet Fission in a Covalently Linked Cofacial Alkynyltetracene Dimer. *J. Am. Chem. Soc.* **2016**, *138*, 617-627.

(37) Fletcher, J. T.; Therien, M. J. Strongly Coupled Porphyrin Arrays Featuring Both π-Cofacial and Linear π-Conjugative Interactions. *Inorg. Chem.* **2002**, *41*, 331-341.

(38) Roy, P. P.; Kundu, S.; Valdiviezo, J.; Bullard, G.; Fletrcher, J. T.; Liu, R.; Yang, S.-J.; Zhang, P.; Beratan, D. N.; Therien, M. J.; Makri, N.; Fleming, G. R. Synthetic Control of Exciton Dynamics in Bioinspired Cofacial Porphyrin Dimers. *J. Am. Chem. Soc.* **2022**, *ASAP Article*: DOI: 10.1021/jacs.1c12889.

(39) Gillgan, A. T.; Miller, E. G.; Sammakia, T.; Damrauer, N. H. Using Structurally Well-Defined Norbornyl-Bridged Acene Dimers to Map a Mechanistic Landscape for Correlated Triplet Formation in Singlet Fission. *J. Am. Chem. Soc.* **2019**, *141*, 5961-5971.

(40) Kaufman, C.; Bialas, D.; Stolte, M.; Würthner, F. Discrete π-Stacks of Prylene Bisimide Dyes within Folda-Dimers: Insight into Long- and Short-Range Exciton Coupling. *J. Am. Chem. Soc.* **2018**, *140*, 9986-9995.

(41) Papadopoulos, I.; Zirzlmeier, J.; Hetzer, C.; Bae, Y. J.; Krzyaniak, M. D.; Wasielewski, M. R.; Clark, T.; Tykwinski, R. R.; Guldi, D. M. Varying the Interpentacene Electronic Coupling to Tune Singlet Fission. *J. Am. Chem. Soc.* **2019**, *141*, 6191-6203.

(42) Zhong, C.; Bialas, D.; Collison, C. J.; Spano, F. C. Davydov Splitting in Squaraine Dimers. *J. Phys. Chem. C*. **2019**, *123*, 18734-18745.

(43) Bialas, D.; Zhong, C.; Wurthner, F.; Spano, F. C. Essential Model for Merocyanine Dye Stacks: Bridging Electronic and Optical Absorption Properties. *J. Phys. Chem. C,* **2019**, *123*, 18654-18664.

(44) Berova, N.; Gargiulo, D.; Derguini, F.; Nakanishi, K.; Harada, N. Unique UV-vis Absorption and Circular Dichroic Exciton-Split Spectra of a Chiral Biscyanine Dye: Origin and Nature. *J. Am. Chem. Soc.* **1993**, *115*, 4769-4775.

(45) Filatov, M. A.; Lebedev, A. Y.; Mukhin, S. N.; Vinogradov, S. A.; Cheprakov, A. V. p-Extended Dipyrrins Capable of Highly Fluorogenic Complexation with Metal Ions. *J. Am. Chem. Soc.* **2010**, *132*, 9552-9554.

(46) Roy, A.; Diers, J.; Niedzwiedzki, D.; Meares, A.; Yu, Z.; Bhagavathy, G. V.; Satraitis, A.; Kirmaier, C.; Ptaszek, M.; Bocian, D.; Holten, D. Photophysical Properties and Electronic Structure of Hydroporphyrin Dyads Exhibiting Strong Through-Bond Electronic Interactions". *J. Phys. Chem. A.* **2022**, *126*, 5107-5125.

(47) Whited, M. T.; Patel, N. M.; Roberts, S. T.; Allen, K.; Djurovich, P. I.; Bradforth, S. E.; Thompson, M. E. Symmetry-Breaking Intramolecular Charge Transfer in the Excited State of *meso*-Linked BODIPY Dyads. *Chem. Comm.* **2012**, *48*, 284-286.

(48) Liu, Y.; Zhao, J.; Iagatti, A.; Bussoti, L.; Foggi, P.; Castellucci, E.; Di Donato, M.; Han, K.-L. A Revisit to the Orthogonal BODIPY Dimers: Experimental Evidence for the Symmetry Breaking Charge Transfer-Induced Intersystem Crossing. *J. Phys. Chem. C.* **2018**, *122*, 2502-2511.

(49) Saki, N.; Dinc, T.; Akkaya, E. U. Excimer Emission and Energy Transfer in Cofacial Boradiazaindacene (BODIPY) Dimers Built in a Xanthene Scaffold. *Tetrahedron*, **2006**, *62*, 2721-2725.

(50) Alamiry, M. A. H.; Benniston, A. C.; Copley, G.; Harriman, A.; Howgego, D. Intramolecular Excimer Formation for Covalently Linked Boron Dipyrromethane Dyes. *J. Phys. Chem. A,* **2011**, *115*, 12111-12119.

(51) Kasha, M. Energy Transfer Mechanism and the Molecular Exciton Model for Molecular Aggregates. *Radiat. Res.* **1963**, *20*, 55-70.

(52) Kasha, M.; Rawls, H. R.; Ashraf El-Bayoumi, M. The Exciton Model in Molecular Spectroscopy. *Pure Appl. Chem.* **1965**, *11*, 371-392.

(53) Knippenberg, S.; Bohnwagner, M. V.; Harbach, P. H. P.; Dreuw, A. Strong Electronic Coupling Dominates the Absorption and Fluorescence Spectra of Covalently Bound BisBODIPYs. *J. Phys. Chem.* **2015**, *119*, 1323-1331.

(54) Meares, A.; Yu, Z.; Bhagavathy, G. V.; Satraitis, A.; Ptaszek, M. Photoisomerization of Enediynyl Linker Leads to Slipped Co-facial Hydroporphyrin Dimers with Strong Through-Bond and Through-Space Electronic Interactions. *J. Org. Chem.* **2019**, *84*, 7851- 7862.

(55) Loudet, A.; Burgess K. BODIPY Dyes and Their Derivatives: Synthesis and Spectroscopic Properties. *Chem. Rev.* **2007**, *107*, 4891-4932.

(56) Ziessel, R.; Harriman, A. Artificial Light-Harvesting Antennae: Electronic Energy Transfer by Way of Molecular Funnels *Chem. Comm.* **2011**, *47*, 611-631.

(57) El-Khouly, M. E.; Fukuzumi, S.; D'Souza, F. Photosynthetic Antenna-Reaction Center Mimicry by Using Boron Dipyrromethene Sensitizers. *ChemPhysChem* **2014**, *15*, 30-47.

(58) Cakmak, Y.; Akkaya, E. U. Phenylethynyl-BODIPY Oligomers: Bright Dyes and Fluorescence Building Blocks. *Org. Lett.* **2009**, *11*, 85-88.

(59) Kusaka, S.; Sakamoto, R.; Kitagawa, Y.; Okumura, M.; Nishihara, H. *meso* Alkynyl BODIPYs: Structure, Properties, p-Extension and Manipulation of Frontier Orbitals. *Chem. Asian. J.* **2013**, *8*, 723-727.

(60) Ahrens, J.; Haberlag, B. Scheja, A.; Tamm, M.; Bröring, M. Conjugated BODIPY DYEmers by Metathesis Reactions. *Chem. Eur. J.* ***2014,*** 20*,* 2901-2912.

(61) Wu, W.; Guo, H.; Wu, W.; Ji, S.; Zhao, J. Organic Triplet Sensitizer Library Derived from a Single Chromophore (BODIPY) with Long-Lived Triplet Excited State for Triplet-TripletAnnihilation Based Upconversion. *J. Org. Chem.* **2011**, *76*, 7056-7064.

(62) Wu, W.; Zhao, J.; Sun, J.; Guo, S. Light-Harvesting Fullerene Dyads as Organic Triplet Photosensitizers for Triplet-Triplet Annihilation Upconversions. *J. Org. Chem.* **2012**, *77*, 5305-5312.

(63) Chase, D. T.; Young, B. S.; Haley, M. M. Incorporating BODIPY Fluorophores into Tetrakis(arylethynyl)benzenes. *J. Org. Chem.* **2016**, *76*, 4043-4051.

(64) Zhang, W.; Sheng, W.; Yu, C.; Wei, Y.; Wang, H.; Hao, E.; Jiao, L. One-pot Synthesis and Properties of Well-defined Butadiynylene-BODIPY Oligomers. *Chem. Comm.* **2017**, *53*, 5318-5321.

(65) Benniston, A. C.; Copley, G.; Harriman, A.; Howgego, D.; Harrington, R. W. Clegg, W. Cofacial Boron Dipyrromethane (BODIPY) Dimers: Synthesis, Charge Delocalization, and Exciton Coupling. *J. Org. Chem.* **2010**, *75*, 2018-2027.

(66) Deschamps, J.; Chang, Y.; Langlois, A.; Desbois, N.; Gros, C. P.; Harvey, P. D. The First Example of Cofacial Bis(dipyrrins). *New. J. Chem.* **2016**, *5835-5845.*

(67) Bröring, M.; Krüger, R.; Link, S.; Kleeberg, C.; Köhler, S.; Xie, X.; Ventura, B.; Flamingi, L. Bis(BF_2)-2,2'-Bidipyrrins (BisBODIPYs): Highly Fluorescent BODIPY Dimers with a Large Stokes Shifts. *Chem. Eur. J.* **2008**, *14*, 2976-2983.

(68) Cakmak, Y.; Kolemen, S.; Duman, S.; Dede, Y.; Dolen, Y.; Kilic, B.; Kostereli, Z.; Yildrim, L. T.; Dogan, A. L.; Guc, D.; Akkaya, E. U. Designing Excited States: Theory-Guided Access to Efficient Photosensitizers for Photodynamic Action. *Angew. Chem. Int. Ed.* **2011**, *50*, 11937-11941.

(69) Montero, R.; Martinez-Martinez, V.; Longarte, A.; Epelde-Elezcano, N.; Palao, E.; Lamas, I.; Manzano, H.; Agarrabeitia, A. R.; Arbeola, I. L.; Ortiz, M. J.; Garcia-Moreno, I. Singlet Fission Mediated Photophysics of BODIPY Dimers, *J. Phys. Chem. Lett.* **2018**, *9*, 641-646.

(70) Qin, Y.; Liu, X.; Jia, P.-P.; Xu, L.; Yang, H.-B. BODIPY-Based Macrocycles. *Chem. Soc. Rev.* **2020**, *49*, 5678-5703.

(71) Kim, T.; Duan, Z.; Talukdar, S.; Lei, C.; Kim, D.; Sessler, J. L., Sarma, T. Excitonically Coupled Cyclic BF_2 Arrays of Calix[8]- and Calix[16]phyrin as Near-IR-Chromophores. *Angew. Chem. Int. Ed.* **2020**, *59*, 13063-13070.

(72) Chen, H.; Shi, X.; Lun, Y.; Xu, Y.; Lu, T.; Duan, Z.; Shao, M.; Sessler, J. L.; Yu, H.; Lei, C. 3,6-Carbazoylene Octaphyrin (1.0.0.0.1.0.0.0) and Its Bis-BF_2 Complex. *J. Am. Chem. Soc.* **2022**, *144*, 8194-8203.

(73) Zhu, Z.; Zhang, X.; Guo, X.; Wu, Q.; Li, Z.; Yu, C.; Hao, E.; Jiao, L.; Zhao, J. Orthogonally Aligned Cyclic BODIPY Arrays with Long-Lived Triplet Excited States as Efficient Heavy-Atom Free Photosensitizers. *Chem. Sci.* **2021**, *12*, 14944-14951.

(74) Xue, S.; Kuzuhara, D.; Aratani, N.; Yamada, H. Vinylene-Bridged Cyclic Dipyrrin and BODIPY Trimers. *Inter. J. Mol. Struct.* **2020**, *21*, 8041

(75) Bergstrom, F.; Mikhalyov, I.; Hagglof, P.; Wortmann, R.; Ny, T.; Johansson, B.-A. Dimers of Dipyrrometheneboron Difluoride (BODIPY) with Light Spectroscopic Applications in Chemistry and Biology. *J. Am. Chem. Soc.* **2002**, *124*, 196-204.

(76) Nguyen, A. L.; Bobadova-Parvanova, P.; Hopfinger, M.; Fronczek, F. R.; Smith, K. M.; Vicente, M. G. H. Synthesis and Reactivity of 4,4-Dialkoxy-BODIPYs: An Experimental and Computational Study. *Inorg. Chem.* **2015**, *54*, 3228-3236.

(77) Vegesna, G. K.; Sripathi, S. R.; Zhang, J.; Zhu, S.; He, W.; Luo, F.-T.; Jahng, W. J.; Frost, M.; Liu, H. Highly Water-Soluble BODIPY-Based Fluorescent Probe for Sensitive and Selective Detection of Nitric Oxide in Living Cells. *ACS Appl. Mater. Interface,* **2013**, *5*, 4107-4112.

(78) Wagner, R. W.; Johnson, T. E.; Li, F.; Lindsey, J. S. Synthesis of Ethyne-Linked or Butadiyne-Linked Porphyrin Arrays Using Mild, Copper-Free, Pd-mediated Coupling Reactions. *J. Org. Chem.* **1995**, *60*, 5266-5273.

(79) Berthelot, J.; Benammar, Y.; Desmazières, B. Solvent Incorporation in Bromination of

Alkynes with Tetrabutylammonium Tribromide in Methanol. *Synth. Commun.* **1997**, *27*, 2865-2876.

(80) Rossi, R.; Bellina, F.; Carpita, A.; Mazzarella, F. Palladium-Mediated Cross-Coupling Reactions Involving 3-Substituted Alkyl (E)-2,3-Dibromopropenoates and Arylzinc or Aryltin Derivatives. *Tetrahedron*, **1996**, *52,* 4095-4110.

(81) Arnett, D. C.; Moser, C. C.; Dutton, P. L.; Scherer, N. F. The First Events in Photosynthesis: Electronic Coupling and Energy Transfer Dynamics in the Photosynthetic Reaction Center from *Rhodobacter Sphaeroides. J. Phys. Chem. B*, **1999**, *103*, 2014-2032.

(82) B. Valeur, *Molecular Fluorescence: Principles and Applications* (Wiley-VCH, 2002).

(83) Johnson, S. G.; Small, G. J.; Johnson, D. G.; Svec, W. A.; Wasielewski, M. R.; Chlorophyll-Porphyrin Heterodimers with Orthogonal π System: Solvent Polarity Dependent Photophysics. *J. Am. Chem. Soc.* **1990**, *112*, 6482-6488.

(84) Kang, H. S.; Esemoto, N. N.; Diers, J.; Niedzwiedzki, D.; Greco, J.; Akhigbe, J.; Yu, Z.; Pancholi, C.; Viswanathan B., G.; Nguyen, J. K.; Kirmaier, C.; Birge, R.; Ptaszek, M.; Holten, D.; Bocian, D. F. Effects of Strong Electronic Coupling in Chlorin and Bacteriochlorin Dyads *J. Phys. Chem. A* **2016**, *120*, 379-385.

(85) Joo, B.; Han, H.; Kim, E.-G., Solvation-Mediated Tuning of the Range-Separate Hybrid Functional: Self-Sufficiency through Screened Exchange. *J. Chem. Theor. Calc.* **2018**, *14*, 2823-2828.

(86) Bhandari, S.; Cheung, M. S.; Geva, E.; Kronik, L.; Dunietz, B. D., Fundamental Gaps of Condensed-Phase Organic Semiconductors from Single-Molecule Calculations using Polarization-Consistent Optimally Tuned Screened Range-Separated Hybrid Functionals. *J. Chem. Theor. Comp.* **2018**, *14*, 6287-6294.

(87) Williams, R. V. Homoaromaticity. *Chem. Rev.* **2001**, *101*, 11850-1204.

(88) Scholes, G. D.; Ghiggino, K. P.; Oliver, A. M.; Paddon-Row, M. N. Through-Space and Through-Bond Effects on Excitation Interactions in Rigidly Linked Dinaphthyl Molecules. *J. Am. Chem. Soc.* **1993**, *115*, 4345-4349.

(89) Jansen, G.; Kahlert, B.; Klärner, F.-G.; Boese, R.; Bläser, D. Intramolecular Electronic Interactions Between Nonconjugated Arene and Quinone Chromophores. *J. Am. Chem. Soc.* **2010**, *132*, 8581-8592.

(90) Paddon-Row, M. N.; Shephard, M. J. Through-Bond Orbital Coupling, the Parity Rule, and the Design of "Superbridges" Which Exhibit Greatly Enhanced Electronic Coupling: A Natural Bond Orbital Analysis. *J. Am. Chem. Soc.* **1997**, *119*, 5355-5365.

(91) Goldshmith, R. H.; Vura-Weis, J.; Scott, A. M.; Borkar, S.; Sen, A.; Ratner, M. A.; Wasielewski, M. R. Unexpectedly Similar Charge Transfer Rates through Benzo-Annulated Bicyclo[2.2.2]octanes. *J. Am. Chem. Soc.* **2008**, *130*, 7659-7669.

(92) Mandal, A. K.; Taniguchi, M.; Diers, J. R.; Niedzwiedzki, D. M.; Kirmaier, C.; Lindsey, J. S.; Bocian, D. F.; Holten, D. Photophysical Properties and Electronic Structure of Porphyrins Bearing Zero to Four *meso*-Phenyl Substituents: New Insight into Seemingly well Understood Tetrapyrroles. *J. Phys. Chem. A,* **2016**, *120*, 9719-9731.

(93) Ohio Supercomputer Center. 1987. Ohio Supercomputer Center. Columbus OH: Ohio Supercomputer Center. http://osc.edu/ark:/19495/f5s1ph73.